Pergamon

Geochimica et Cosmochimica Acta, Vol. 65, No. 5, pp. 715–727, 2001

0016-7037/01 $20.00 + .00

PII S0016-7037(00)00530-5

Early development of Al, Ca, and Na compositional gradients in labradorite leached in pH 2 HCl solutions

H. W. NESBITT[1,*] and W. M. SKINNER[2]

[1]Department of Earth Sciences, University of Western Ontario, London, Ontario, N6A 5B7, Canada
[2]Ian Wark Research Institute, University of South Australia, Mawson Lakes, South Australia, 5095, Australia

(*Received February* 9, 1999; *accepted in revised form August* 17, 2000)

Abstract—Labradorite reacted with HCl solution (pH = 2.0) develops leached layers extending to about 500 Å depth after 12 h leaching, and to 1500 Å depth after 143 h leaching. Accurate Al, Ca, and Na compositional depth profiles were measured using x-ray photoelectron spectroscopy (XPS), with compositional accuracy of about 10% and depth resolution of about 50 Å. XPS analyses of pristine K-feldspar and labradorite surfaces yield Ca, Al, Si, and O analyses within about 5% of electron microprobe results. Alkali element analyses are inaccurate due to preferential sputtering or mobility induced by fracture. The accurate compositional depth profiles yield well constrained diffusion coefficients and moving boundary velocities for Ca and Al. Na, Ca, and Al compositional gradients change character after about 2 days of leaching, from a convex upward hyperboloid to a sigmoid shape. Thereafter, the feldspar diffusion front is clearly separated from the surface (where silica dissolution occurs), with the diffusion front migrating into the feldspar at about 4×10^{-11} cm/s. Al diffuses down the compositional gradient at about 2.5×10^{-17} cm^2/s and Ca diffuses almost twice as fast (4.0×10^{-17} cm^2/s). The solution–solid interface and active leaching zone are separated (after 2 days) by a Si-rich zone virtually devoid of Na, Ca, and Al. Diffusion rates through this Si-rich overlayer may be very rapid and approach rates observed in aqueous solutions. Diffusive release of Ca and Al from labradorite cannot be modelled accurately with mathematical solutions where diffusion through homogeneous media is assumed. During leaching, Ca and Al apparently diffuse by "jumping" to, and residing on, previously vacated structural sites of the feldspar. The probability of Ca and Al migrating towards solution consequently is greater than their probability of migrating towards pristine plagioclase, primarily because there are many more "vacant" sites in the leached zone than in pristine plagioclase. Diffusion is inhomogeneous and "impeded" in the direction of the pristine feldspar. *Copyright © 2001 Elsevier Science Ltd*

1. INTRODUCTION

Surface analytical studies over the last 10 years have demonstrated that feldspars leached for prolonged periods in strong acids produce a siliceous overlayer largely depleted of Al, Ca, and Na (Casey et al., 1988; 1989; Muir et al., 1989; 1997; Nesbitt et al., 1991; Schweda et al., 1997; Adriaens et al., 1999). These studies were conducted using primarily dynamic secondary ion mass spectrometric (SIMS) and Rutherford backscattering (RBS) techniques. Long leaching periods generally were required to overcome problems inherent to the analytical techniques. Specifically, dynamic SIMS measurements generally cannot provide reliable analyses of the top 50–100 Å of surfaces (Nesbitt et al., 1991) because time is required to achieve thermal and compositional steady state at the sputtered surface. RBS has a depth resolution no better than about 200 Å associated with feldspar leaching (Casey et al., 1988; 1989) so that leached layers thinner than this cannot be accurately analyzed. There are consequently no detailed studies designed to measure directly the compositional changes at feldspar surfaces during the early stages of leaching.

The first objective of this study is to document the early evolution of compositional gradients in a feldspar leached by inorganic acids (here labradorite leached by HCl solution of pH = 2.0). Although HCl was used in these experiments, the profiles and implications are likely to apply to all plagioclase compositions leached by all inorganic acids provided the ligand does not form a strong surface complex (Muir and Nesbitt, 1997). The studies are relevant to feldspar dissolution during the very early evolution of the earth where carbon dioxide partial pressures of the atmosphere may have been much greater, and rainwater contained much more H_2CO_3 than today. The results and implications have bearing on natural feldspar weathering in all highly acidic regimes.

A second objective is to identify the various diffusional regimes that may develop during dissolution, and to gain greater insight into diffusional processes affecting feldspar dissolution. X-ray photoelectron spectroscopy (XPS) was employed to collect compositional depth profiles of leached layers because depth resolution and quantitative elemental analyses are much more accurate than can be obtained by either SIMS or Rutherford backscattering techniques (Briggs and Seah, 1990). Although compositional gradients obtained by SIMS were used to estimate diffusion coefficients of Al and Ca (Nesbitt et al., 1990; Schweda et al., 1997), values derived from the XPS data are much more accurate.

2. METHODS AND RESULTS

2.1. Sample Properties and Preparation

Labradorite fragments measuring about 2 cm on a side were used for the study. They were transparent and weakly iridescent. The samples, collected from Cassino, New South Wales, Australia, were obtained from the South Australian Museum through Dr. A. Pring. Ten electron microprobe analyses yielded an average elemental composition (based on eight oxygen) of Si = 2.57 (σ = 0.004); Al = 1.41 (σ = 0.004);

* Author to whom correspondence should be addressed.

Ca = 0.49 (σ = 0.003); Na = 0.47 (σ = 0.006); K = 0.03 (σ = 0.001); Fe = 0.01 (σ = 0.001). The average of these elements was 4.98 (σ = 0.006).

The samples were cleaved along (001) with a knife to produce smooth cleavage faces. Only cleavage surfaces devoid of steps over areas of at least 4 × 4 mm were used for the experiments. For each experiment a cleavage fragment was placed in a stirred beaker containing 1 L of HCl solution (pH = 2.0 ± 0.1). Some experiments were conducted containing two similarly sized fragments for duplicate analysis. Cleavage fragments were reacted with solution for 12, 26, 48, 70, and 143 hours. The solution was completely replaced by a fresh batch of pH 2 solution every 12 hours to prevent excessive buildup of cations in solution.

Each fragment was reacted for a specified period after which it was removed from solution, carefully blotted with Kimwipe, and immediately placed in the XPS introduction chamber to allow any remaining solution to be evaporated. It was then cooled to near liquid nitrogen temperatures until the vacuum was sufficient to allow transfer to the analytical chamber. Cooling was employed to limit thermal effects (e.g., diffusion and restructuring) and most importantly to limit water loss from the leached zones.

Analysis of the pristine cleavage surface was accomplished by introducing the cleaved fragments into the introduction chamber immediately after cleavage. XPS surface analysis and compositional depth profiles of the cleavage surfaces were subsequently collected.

2.2. Analytical Equipment and Conditions

Compositional depth profiles were collected using x-ray photoelectron spectroscopy (XPS) for the following reasons. XPS analyses can be made reasonably accurate (errors within about 5% of the value) by use of appropriate sensitivity factors. These are tabulated or can be measured using standards. Techniques previously used to document compositional profiles in leached feldspars are at best semiquantitative, and generally qualitative. As well, the effects of sample charging are readily monitored by XPS, with appropriate compensation made to minimize the effects of charging.

XPS spectra were recorded using a PHI Model 5600 hemispheric electron spectrometer with pass energy set at 18 eV for surface analysis and 26.8 eV during depth profiles. A nonmonochromatized Al K_α x-ray source operating at 300 W was used. The main chamber pressure during analysis was circa 10^{-9} torr. The spectrometer energy scale was calibrated using the Fermi edge and the $3d_{5/2}$ line (367.9 eV) for silver, whereas the retardation voltage was calibrated noting the positions of the Cu $2p_{3/2}$ (932.7 eV) and Cu $3p_{3/2}$ (75.1 eV) peaks. The resultant position of the C 1*s* photopeak due to adventitious hydrocarbon was found at 284.8 eV. All XPS measurements were recorded at a take-off angle of 45°. Atomic concentrations for each element were determined from photopeak areas and listed sensitivity factors (Wagner et al., 1976) available within both the instrument and stand-alone data analysis software. A liquid nitrogen cooled stage was employed for all surface and depth profile measurements to minimize the possibility of X-radiation-induced thermal diffusion and water loss during analysis.

Compositional depth profiling was accomplished by sequential sputtering using a 3 kV Ar ion beam. The ion beam was rastered over a 4 × 4 mm area and analyses were taken from a 1 × 1 mm area in the center of the sputter crater. The sputter rate of labradorite was measured by atomic force microscopy on several 3000 s sputter craters on freshly cleaved samples, and was determined to be 17 Å per minute. This sputter rate compared favorably with that of thermally grown SiO_2 on Si under the same beam conditions. The major peaks monitored during depth profiling included C 1s, O 1s, Si 2p, Al 2p, Ca 2p, and Na 2s. The Na 2s line was selected for this study rather than the Na 1*s*, as its escape depth lay in the same range as the other lines of importance.

3. PRISTINE SURFACES AND ANALYTICAL LIMITATIONS

3.1. Surface Analyses

Two analyses of an unleached K-feldspar are plotted in Figure 1a, and demonstrate analytical precision. With carbon excluded, the average of the two K-feldspar surface analyses was O = 60.70 at .%; Si = 22.80%; Al = 8.05%; K = 6.17%, and Na = 2.29%. These compare well with the idealized composition $(K, Na)_1Al_1Si_3O_8$ which yields 61.5% oxygen, 23.1% Si, and 7.7% Al and K + Na (atomic basis). The XPS analysis of oxygen is in error by 1.4%, Si by 0.5%, and Al by 4.7%.

The sum of K + Na is 8.46, and exceeds the ideal value by 10%. The high Na content is attributable to an interference. An Al 2*p* satellite line overlaps the Na 2s peak producing an overestimate of the Na content. The Al 2*p* satellite is approximately 12% that of Al 2*p* main line (Wagner et al., 1976) and the appropriate correction yields 1.41% Na. With this value, K + Na is 7.58% and close to the ideal value (7.7%). The corrected XPS analysis yields the composition $K_{0.81}Na_{0.19}Al_{1.06}Si_{3.01}O_{8.0}$. The XPS technique consequently provides reasonable alkali feldspar *surface* analyses using conventional yield factors (Wagner et al., 1976), once correction to the Na 2s signal is made.

3.2. Depth Profiles

The O, Si, and Al signals of K-feldspar are effectively independent of depth (Fig. 1a). The K 2*p* signal, however, decreases systematically with depth to achieve a constant value after 800 seconds of sputtering (200 Å depth). Apparently potassium is preferentially sputtered, thus complicating the interpretation of compositional profiles for this element.

Si and O: The oxygen compositional depth profile of a pristine labradorite cleavage face (Fig. 1b) is essentially flat, with values near the ideal composition (61.54%) at all depths. Although the Si signal is effectively independent of depth (Fig. 1b), the two surface analyses yield higher concentrations. The reason is uncertain.

Al, Ca, and Na: The Al signal (Fig. 1b) is slightly depressed between surface and about 100 Å depth, but is constant at greater depth. The Ca signal behaves similarly. The Na profile is enhanced in the topmost 200 Å and may result from preferential sputtering or from migration of Na to the surface induced by cleavage.

There is an antipathetic relationship between Na and Ca and between Si and Al, and a sympathetic relation between Ca and Al. These relations are expected where plagioclase composition is more sodic near the surface and more calcic beyond about 200–300 Å depth. Compositional zoning (Bøggild intergrowths) on this scale is common in labradorite (Smith and Brown, 1987). Regardless of the explanation for the Al and Ca variations in the near surface, the results of Figure 1b demonstrate that there is minimal Al and Ca preferential sputtering.

3.3. Molar Proportions

Al + Si should equal 4.0 (molar basis) in all feldspars when normalized to 8 mol oxygen. The sum for K-feldspar is close to this (Fig. 1c), but is near 4.3 in labradorite (Fig. 1d). Comparison of Ca, Si, and Al ratios suggests that Al content is consistently too high in labradorite by about 0.3 mol (per 8 mol oxygen). The Al XPS yields therefore may have to be corrected for the labradorite matrix. The sum of Ca and Na is low for labradorite and as for K in K-feldspar, low Na yields may be due to preferential sputtering.

Figure 1 shows that reasonable elemental analyses can be

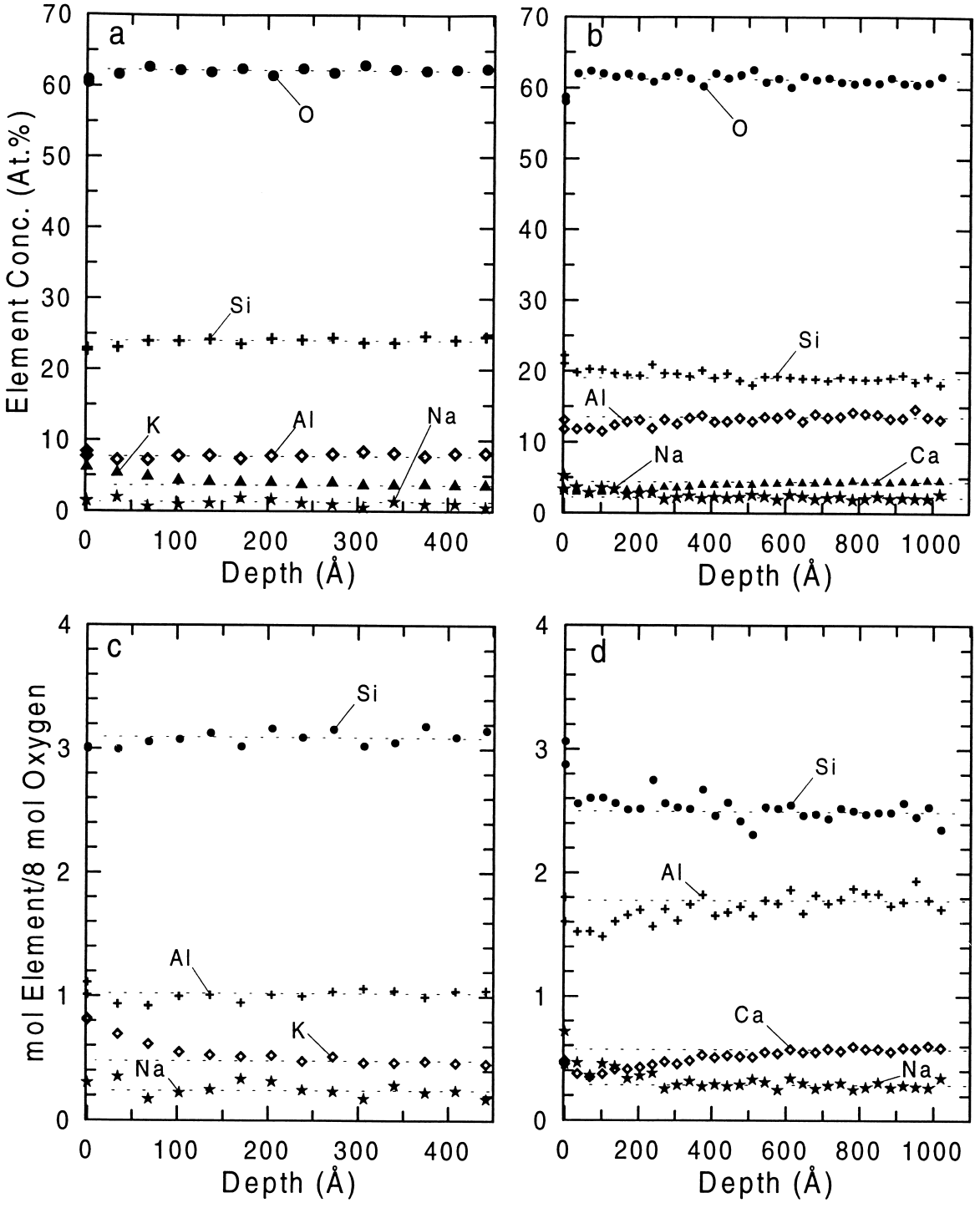

Fig. 1. XPS compositional depth profiles of unreacted feldspar cleavage (001) surfaces. (a) Compositional profile of K-feldspar showing the atomic percents of K, Na, Al, Si, and O. The idealized composition is 7.70% K + Na, 7.70% Al, 23.08% Si, and 61.54% O. (b) Compositional depth profile of labradorite. Its actual composition from microprobe analyses is 3.62% Na, 3.77% Ca, 10.85% Al 19.77% Si, and 61.54% O. (c) The K-feldspar depth profile analyses of (a) normalized to 8 mol of oxygen atoms [idealized composition, $(K + Na)_1Al_1Si_3O_8$]. (d) The labradorite depth profile analyses of (b) normalized to 8 mol of oxygen atoms [composition is $(K + Na + Ca)_1(Al + Fe)_{1.43}Si_{2.57}O_8$ where Fe is taken to substitute for Al].

obtained from smooth cleavage faces of feldspars. Analytical problems are associated with sputtering the alkali metals, and with slight overestimate of Al contents of labradorite. Even with these problems, the XPS analytical results are far superior to SIMS or RBS analyses. In fact, these XPS results approach electron microprobe accuracy for the cations and provide much better oxygen analyses than can be obtained by electron microprobe techniques. Arguments which follow are based primarily upon Si, Al, and Ca compositional depth profiles.

4. EVOLUTION OF COMPOSITIONAL GRADIENTS

4.1. Formative Stage

The compositional gradients for Ca and Al produced by 12 h to 48 h leaching (Fig. 2) display a convex "upward" hyperboloid aspect. Concentrations are low at the surface and increase monotonically with depth toward pristine labradorite values. Si, by contrast, displays high values in the near surface but decreases in abundance towards pristine labradorite values at depth. These results demonstrate that Al and Ca (and Na, as discussed subsequently) are preferentially leached in the near surface and that there is residual enrichment of Si in the leached zone. After a few tens of hours of leaching, the near surface is largely depleted in Ca and Al (plus Na), leaving a siliceous overlayer in which the ratio Si:O approaches 1:2 (e.g., SiO_2).

The active leaching zone extends to about 500 Å after 12 h to 26 h leaching, and to about 700 Å depth after leaching for about 2 days. These general trends were previously observed in long-term leaching of feldspars (Schweda et al., 1997; Nesbitt et al., 1990; Casey et al., 1988; 1989; Muir et al., 1990) and were interpreted to represent preferential leaching of Al, Ca (and Na), and residual enrichment in Si in the leached layer. There has been, however, no previous documentation of the early stages in development of the profiles.

4.2. Advanced Stage

With continued reaction the zone of active leaching extends to about 750 Å and 1200 Å depth in the 70 h and 143 h leached samples (Fig. 3). A distinctive Si-rich zone is well established and extends from surface to about 100 Å deep at 70 h leaching and to about 250 Å depth with 143 h leaching. Beneath the Si-rich zone, the profiles for both metals assume a sigmoid shape extending some 400 Å beyond the Si-rich zone into both experiments (Fig. 3). Furthermore, the sigmoid profile migrates to greater depth with time, as apparent by comparing the 70 h and 143 h results. A steady state should be established eventually, where surface dissolution of the Si enriched layer and diffusion from the advancing leaching front keep pace, thus establishing a constant thickness for the Si-rich surface layer and a steady state compositional depth profile of unchanging depth and character (sigmoid). The data of Muir et al. (1990) indicate that steady state is achieved before 60 days of leaching in pH 3.5 solutions.

Surface Si is near 3.6 mol (per 8 mol of oxygen) after 12 h leaching. It increases to near 4 mol after 26 h leaching and is maximum (5 mol) at 70 h leaching. The limiting Si:O ratio is 1:2 for SiO_2 and must be lower for hydrated or hydroxylated forms of SiO_2. The analyzed Si:O ratios indicate a slight excess of Si in the surface region (Fig. 3), which may reflect minor preferential sputtering. More likely, however, is that the sensitivity factors for the leached layer are slightly different than for pristine feldspar.

5. ANALYSIS OF PROFILES PRODUCED DURING ADVANCED LEACHING

5.1. General Features

The concentrations of Al and Ca for 26 h, 70 h, and 143 h leaching have been normalized to their concentrations in the pristine plagioclase (Al° and Ca°) and the ratios (Al/Al° and Ca/Ca°) are plotted as a function of depth in Figure 4. The sigmoid profiles for 70 h and 143 h leaching display an unusual aspect near the leaching front. Considering the 143 h experiment, the Al profile at depths greater than about 625 Å define a shallow, near-linear slope rather than being convex upward as expected of a sigmoid profile (Fig. 4a). This characteristic is also apparent in the 70 h experiment. This near-linear trend suggests that diffusional properties near the leaching front (region close to pristine feldspar) are somewhat different from those at shallower depths (0 to 625 Å depth). These aspects are investigated quantitatively to ascertain the reason for the shallow slope.

5.2. Mathematical Simulation

Formulation: The compositional gradients obtained after leaching for 26 h, 70 h, and 143 h (Fig. 4) migrate from the surface region towards the bulk, and sigmoid gradients are produced, as reaction progresses. These characteristics are consistent with diffusion involving a moving boundary, analytical solutions for which are well established (Crank, 1957). An appropriate solution to the differential diffusion equation is provided by Danckwerts (1953):

$$C_i/C_i^0 = \{\mathrm{erfc}[(x - Vt)/(2(D_i t)^{1/2})]\}/2, \qquad (1)$$

where C_i is the concentration of "i," C_i^0 is the initial concentration of "i" in the material of interest (here pristine labradorite), erfc is the error function complement, x is distance, V is the velocity with which the moving boundary migrates, and t is time (Danckwerts, 1953).

Qualitative aspects are shown in Figure 5 where two media, A and B, are distinguished for convenience of modeling. The interface (boundary) between them is by definition, located at the value $C_i/C_i^0 = 0.5$. Conditions required for using Eqn. (1) are (1) the two media are homogeneous with respect to diffusion; (2) the diffusion coefficients of "i" are identical in the two media; (3) the velocity with which the boundary separating A and B migrates is constant over time; (4) the diffusing component "i" initially resides only in medium B (Fig. 5); (5) constituents removed from medium B are retained by medium A. With these restrictions, element "i" diffuses from B into A, where the constraints of mass balance and identical diffusion coefficients in A and B, ensure production of a sigmoid diffusion profile which is symmetric about the point $C_i/C_i^0 = 0.5$ (center of symmetry or inversion point). This symmetry element and the mass balance for "i" are used to calculate the diffusion profiles for negative values of $(x - V_t)$. Qualitative changes to the compositional profile of "i" over time are illustrated in Figure 5a where the interface is stationary.

The boundary between these two media may migrate while

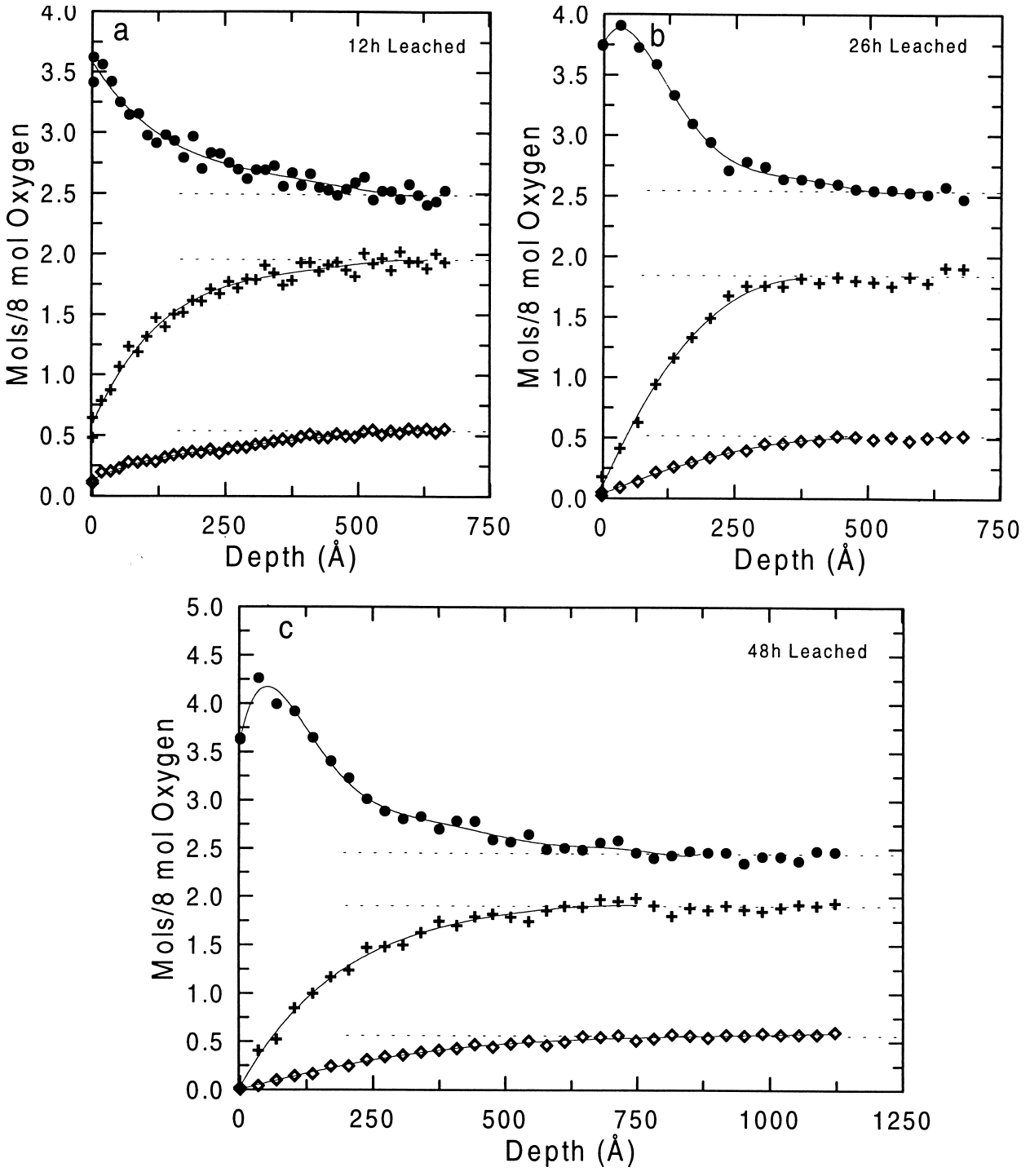

Fig. 2. XPS compositional depth profiles collected from labradorite (001) cleavage surfaces leached for 12 h (a), 26 h (b), and 48 h (c) in HCl solution of pH = 2.0. Dots represent Si (mol), crosses represent Al (mol), and diamonds represent Ca (mol). The curves are polynomial fits to the data. The compositions at each depth were cast as mols and normalized to eight oxygen atoms. Silica (SiO_2) has four Si atoms per eight oxygen atoms and labradorite has a total of five cations per eight oxygen atoms.

component "*i*" diffuses from medium *B* into *A*. Sigmoid profiles are still produced and remain centered on the boundary (with C_i/C_i^0 as inversion point, Fig. 5b). Note that in both Figures 5a and b, the boundary separating the two media is, by definition, always located at $C_i/C_i^0 = 0.5$ on the compositional gradient. This allows for a precise, formal definition of the position of the boundary as it migrates. Figure 5b illustrates qualitative changes to the shape and position of a profile over time.

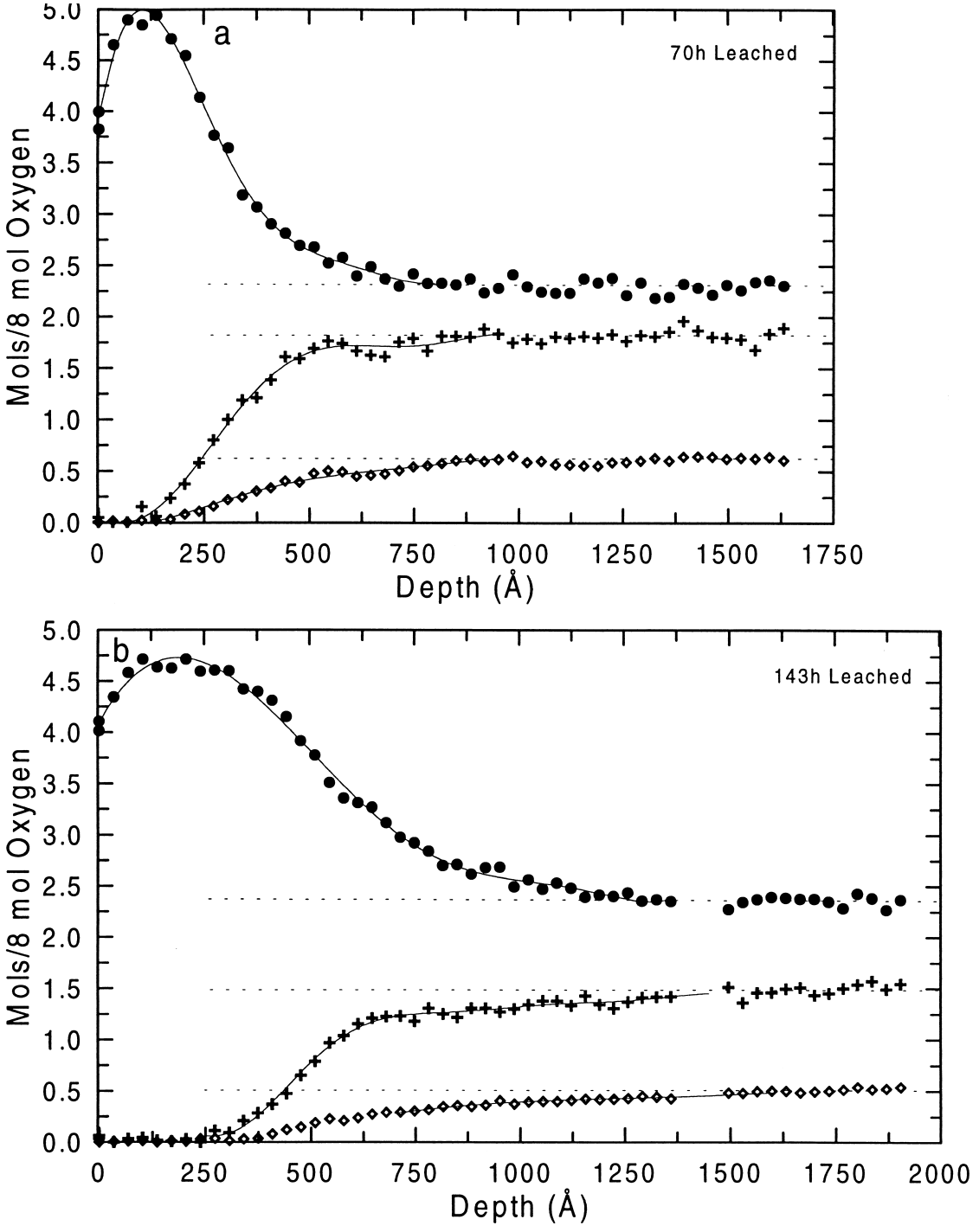

Fig. 3. XPS compositional depth profiles collected from labradorite (001) cleavage surfaces leached for 70 h (a) and 143 h in HCl solution of pH = 2.0. Symbols and other information is provided in the caption to Figure 2.

Considering medium *B* to be pristine labradorite and medium *A* to be the Si-rich zone, Eqn. (1) is applicable to the experimental data of Figure 4 as long as the amount of diffusing element "*i*" (e.g., Al) lost to solution is small compared to the initial mass of "*i*" in medium *B* (i.e., most "*i*" lost from *B* resides in *A*). If the diffusion or velocity coefficient of the interface varies appreciably (within the media) or with time, the equation will not reproduce the shape of the profiles or their rate of migration.

5.3. Application to Al and Ca Profiles

The curves of Figure 4a were calculated using Eqn. (1) with Al diffusion coefficient equal to 2.5×10^{-17} cm^2/s, and with

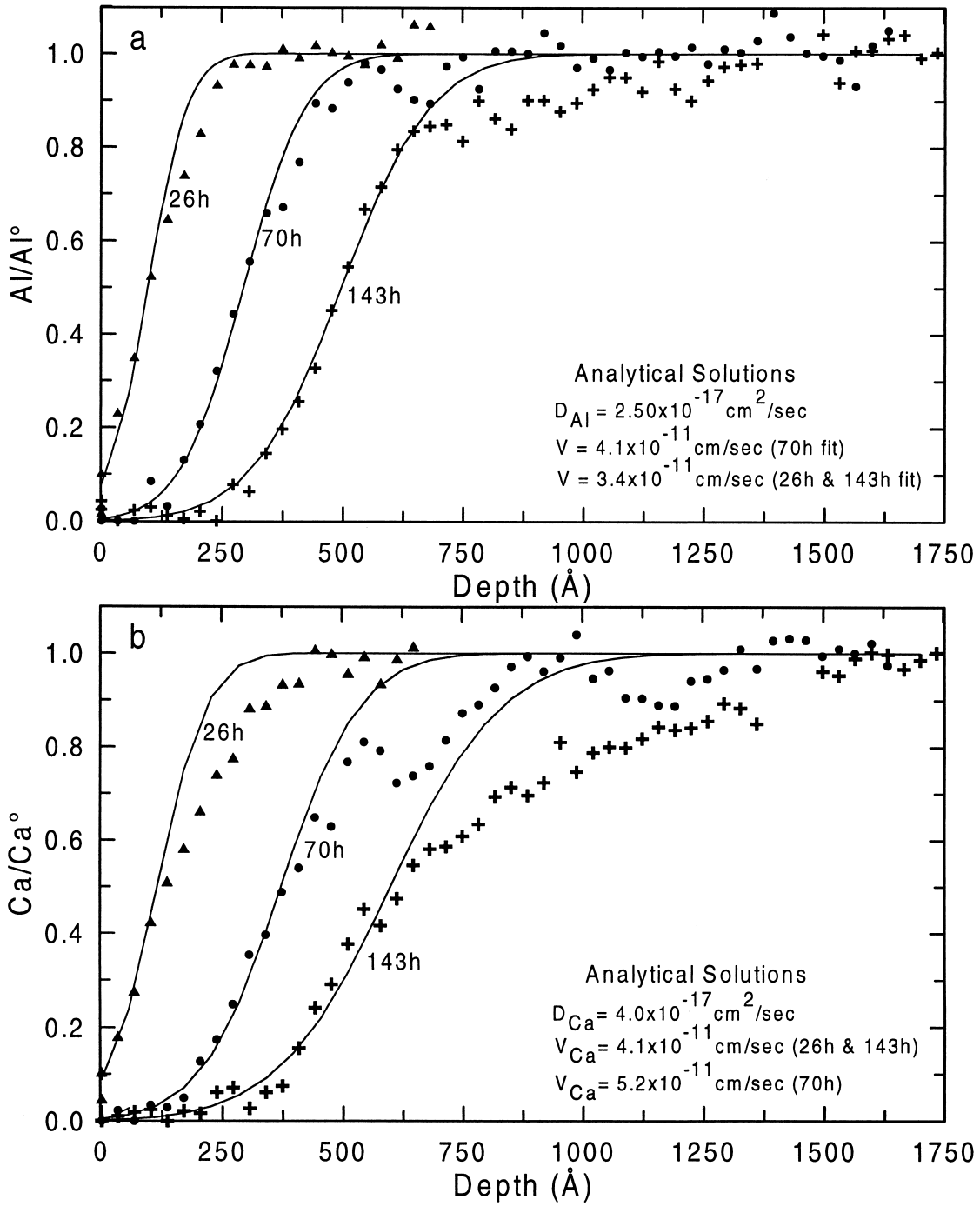

Fig. 4. Schematic diagrams showing changes to the compositional gradient of a component as it diffuses from medium *B* into medium *A*. The ordinate is concentration ratio (C_i/C_i^0). The abscissa is distance (x), with positive and negative values of x determined with reference to the position where $x - V_t = 0$ for each concentration gradient (point where $C_i/C_i^0 = 0.5$). The diffusion coefficients are the same in the two media. (a) The situation where the interface or boundary separating the media is fixed (position does not change with time). (b) The situation with a moving boundary where the interface or boundary migrates into medium *B* as a function of time.

the boundary moving at an average velocity of 3.7×10^{-11} ($\pm 0.4 \times 10^{-11}$) cm/s (see Fig. 4a, inset). With these values the simulation is remarkably successful at reproducing both the sigmoid shape and the rate of migration of the gradients; at 26 h the boundary (Al/Al° = 0.5) is near 100 Å, at about 300 Å after 70 h and at 500 Å after 143 h. The correspondence with experiment demonstrates that migration of the boundary is effectively constant.

The shape of each profile is also reasonably modelled except for a discrepancy at Al/Al° values greater than about 0.8 (Fig.

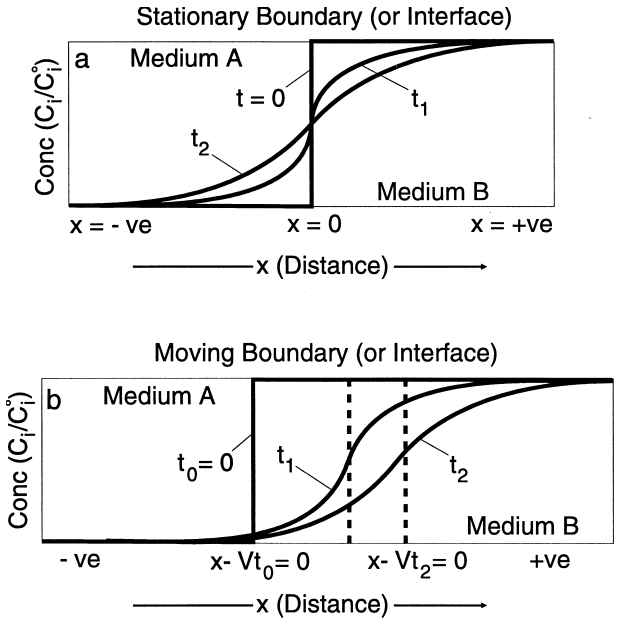

Fig. 5. XPS Al compositional depth profiles of labradorite (001) cleavage surfaces leached in HCl solution of pH = 2.0 for 26 h (triangles), 70 h (dots), and 143 h (crosses). The ordinate (C_{Al}/C^0_{A1}) represents normalized Al compositions for each depth profile of Figures 2 and 3 where normalization is to the Al composition of pristine labradorite. (a) Simulations of the Al gradients, using Eqn. (1) are illustrated as solid curves. Coefficients for the simulations are provided on the diagram. (b) Simulations of the Al gradients, using Monte Carlo calculations, are illustrated by the segmented lines joining the small dots.

4a). At values greater than 0.8, the data plot systematically below the curves in the region nearest the leaching front. Because the calculation successfully simulated the position of the moving boundary, the discrepancy likely is associated with a changed Al diffusion coefficient at the leaching front.

These conclusions also hold for the Ca data (Fig. 4b). The rate of migration of the boundaries is reasonably reproduced using a velocity of 4.7×10^{-11} ($\pm 0.5 \times 10^{-11}$) cm/s. The data, however, deviate from the predicted trends for Ca/Ca° values greater than about 0.6 (Fig. 4b). This comparison confirms that the rate of migration of the boundary is effectively constant but that the diffusion coefficient near the leaching front is different from that at shallower depths.

5.4. Simulation Compared with Other Results

The Ca boundary velocity coefficient (V) is about 25% greater than the Al velocity coefficient. Also, the Ca diffusion coefficient is about 60% greater than the Al coefficient. These results are consistent with the findings of Muir and Nesbitt (1992) who documented Ca and Al profiles in labradorite leached for much longer periods where they observed that Ca was released in advance of Al during leaching.

The calculated diffusion coefficients of Al and Ca in the leaching zone are, respectively, 2.5×10^{-17} and 4.0×10^{-17} cm^2/s. These are comparable to diffusion coefficients of K (5.9×10^{-17} cm^2/s) and Na (8.2×10^{-17} cm^2/s) in alkali silicate glasses (Frischat, 1975). The agreement with the SIMS results and the similarity in diffusion coefficients obtained by different techniques indicate that the diffusion and velocity coefficients are reasonable, validating this approach to modeling the data.

5.5. Limitation of the Analytical Solution

As already noted, the inability of the simulation to reproduce the compositional profiles in the region close to the leaching front suggests that the diffusion coefficient near the leaching front is different from that at shallower depths. The media (A and B), however, must be homogeneous with respect to diffusion for the Danckwerts equation [Eqn. (1)] to be applicable. Stated differently, application of Eqn. (1) to feldspar diffusion requires a diffusing atom to have equal probability to "jump" to *any* adjacent site regardless of the direction of the jump (Kofstad, 1972, p. 71). This condition is not met at the leaching front if Al (Ca or Na) resides on structural sites and jumps *only* to adjacent structural sites.

As explanation, consider medium B as a one-dimensional lattice (Fig. 6a) where all sites initially are occupied by element "i" (Al for example). Beyond the leftmost atom of "i" is medium A which contains sites on which "i" may reside, but which are empty. At initiation of diffusion, the atom at the interface (in B) can migrate (jump) to the left (into A), but it *cannot* "jump" to the right because the site immediately to its right is occupied. At the interface between A and B, and even after extended diffusion, all sites are occupied to the right of the "diffusion front" (Fig. 6b, atom on the site labeled A) but unoccupied sites exist to its left, thus impeded diffusion always occurs at the diffusion or leaching front.

Impeded diffusion does not, however, occur in the extensively leached, Si-rich zone of the near surface of feldspars because there are a near equal number of vacant structural sites on all sides of an atom in this zone (e.g., Fig. 6c, atom "B"). Conventional analytical solutions [Eqn. (1)] are consequently applicable to the Si-enriched zone and to the part of medium B near the interface, thus explaining the success of Eqn. (1) in reproducing the experimental data in these regions. Aspects of this have been addressed in the metallurgical literature by introduction of a correlation coefficient (Borg and Dienes, 1992, pp. 461, 471).

6. EVIDENCE FOR IMPEDED DIFFUSION IN THE ACTIVE LEACHING ZONE

6.1. Monte Carlo Simulation of Al Profiles

Methodology: Although diffusion may proceed via lattice sites or via dislocations (Shewmon, 1963; 1969; LeClaire and Rabinovitch, 1984), the complete leaching of Na, Ca, and Al from the near surface to produce a Si-rich zone indicates that lattice diffusion is of paramount importance in acidic leaching of labradorite. A 50×400 two-dimensional lattice was considered, with a boundary separating the first 200 columns from the second 200 columns, with all sites being identical. Initially all sites of the first 200 columns were vacant and all sites on the second 200 columns were occupied by atoms of type "A" (Fig. 6d). Each Monte Carlo trial involved a jump from one lattice site to another, provided the site to which an atom would jump was vacant. Only left and right jump directions were considered

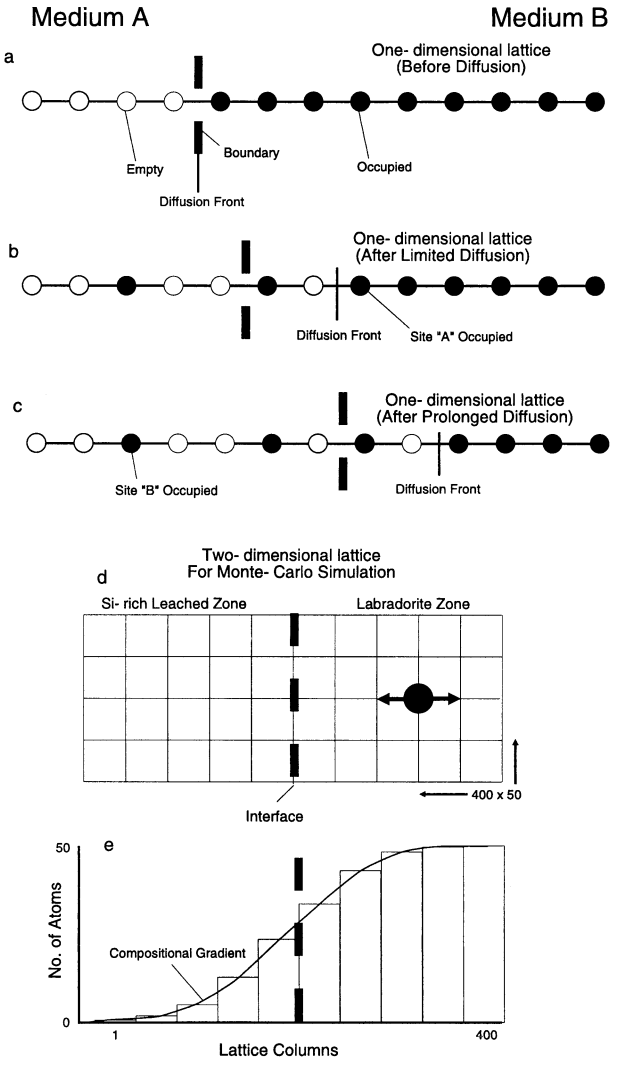

Fig. 6. Schematic illustration of impeded diffusion associated with diffusive "jumps" from one lattice site to another. (a) All lattice sites of medium *B* are occupied, all *A* are empty. (b) A few sites on *B* are vacant near the interface but most are occupied at the leaching front. (c) An ion in medium *A* (e.g., leached zone) has equal probability to diffuse (jump) in either direction. (d) illustrates graphically the Monte Carlo model for diffusion of atoms on lattice sites. (e) illustrates the result of the Monte Carlo simulation where the atoms occupying sites in each lattice "column" are summed to give a discrete compositional gradient in histogram form.

(Fig. 6d, represented by a large dot with arrows) because jumps in a vertical direction had no effect on the compositional gradient here calculated. A random number between 0 and 1 was generated. If the random number was greater than 0.5 the atom jumped to the left, otherwise it jumped to the right. Once jump direction was determined, the jump was successful if the appropriate site was unoccupied, otherwise no jump occurred. Atoms of column 200 were not allowed to "jump" out of the lattice (to the right in Fig. 6d).

Increased leaching time was simulated by increasing the number of Monte Carlo trials undergone by each atom in proportion to the increased time of leaching. Monte Carlo compositional gradients were determined by summing the atoms in each of the lattice columns to obtain an histogram depicting the gradient (Fig. 6e). The Monte Carlo gradient then was scaled to duplicate the experimental gradient at $C_i/C_i^0 = 0.5$, the position of the interface, from which was obtained the value for the "lattice constant" (interatomic distance of Fig. 6c) and the appropriate scale factor for depth. Last the number of atoms in each lattice column (Fig. 6e) was summed and normalized to the total number of lattice sites in the column (50, Fig. 6d) to obtain C_i/C_i^0. The simulated, profiles were then plotted (e.g., Fig. 7).

Comparison with Al and Ca XPS data: Monte Carlo simulations yield discrete values which are illustrated in Figure 7 as straight line segments joining small dots. Comparison of Figure 7a with Figure 5a demonstrates the Monte Carlo simulations for 26 h, 70 h, and 143 h experimental Al data are as good as Eqn. (1) in the Si-enriched zones (Al/Al° < 0.8) and are much better than Eqn. (1) in the region of the leaching front (Al/Al° > 0.8). The successful Monte Carlo simulations provides strong evidence that diffusion is impeded towards the pristine labradorite (relative to diffusion towards solution). It also suggests that Al diffusion near the leaching front is via structural sites (perhaps tetrahedral) rather than via interstitial sites because the latter type is available in both pristine labradorite and the leached zone.

The analytical solution [Eqn. (1)] and the Monte Carlo simulation were also applied to the Ca profiles (Fig. 7b) with conclusions being identical to those derived from application to the Al profiles. Both simulations reproduced the concentration gradients in the Si-enriched zone for Ca/Ca° less than 0.5. Above this value the Monte Carlo simulation was more accurate, although as shown (Fig. 7b) even the Monte Carlo simulation was somewhat inaccurate at high values of Ca/Ca°. Undoubtedly Ca suffers impeded diffusion near the diffusion front, hence the near linear gradient in this region. Diffusion is, however, somewhat more rapid towards solution than predicted by even the Monte Carlo simulation. Although this aspect requires additional study, one explanation may be that Ca may "jump" to more than one type of structural site, thus enhancing diffusion towards solution.

7. SIMULATION OF THE INITIAL STAGE OF AL LEACHING

7.1. Mathematical Simulation

The moving boundary solution is inapplicable to the initial stage of leaching primarily because the mass balance constraint is violated. A solution with stationary boundary is, however, applicable. An appropriate analytical solution is (Crank, 1957, p. 30):

$$C_i/C_i^0 = \mathrm{erf}[\,x/(2(D_i t)^{1/2})],$$

where erf is the error function (erf = 1 erfc). Other symbols are as for Eqn. (1). Equation (2) is applicable as long as Al(aq) concentrations adjacent to the feldspar surface are more than about 100 times lower than the abundance in the feldspar (molar basis).

Equation (2), with a diffusion coefficient of 2.5×10^{-17} cm^2/s (derived from simulation shown in Fig. 4) was used to simulate the 12 h and 48 h experimental results (Fig. 8a). The

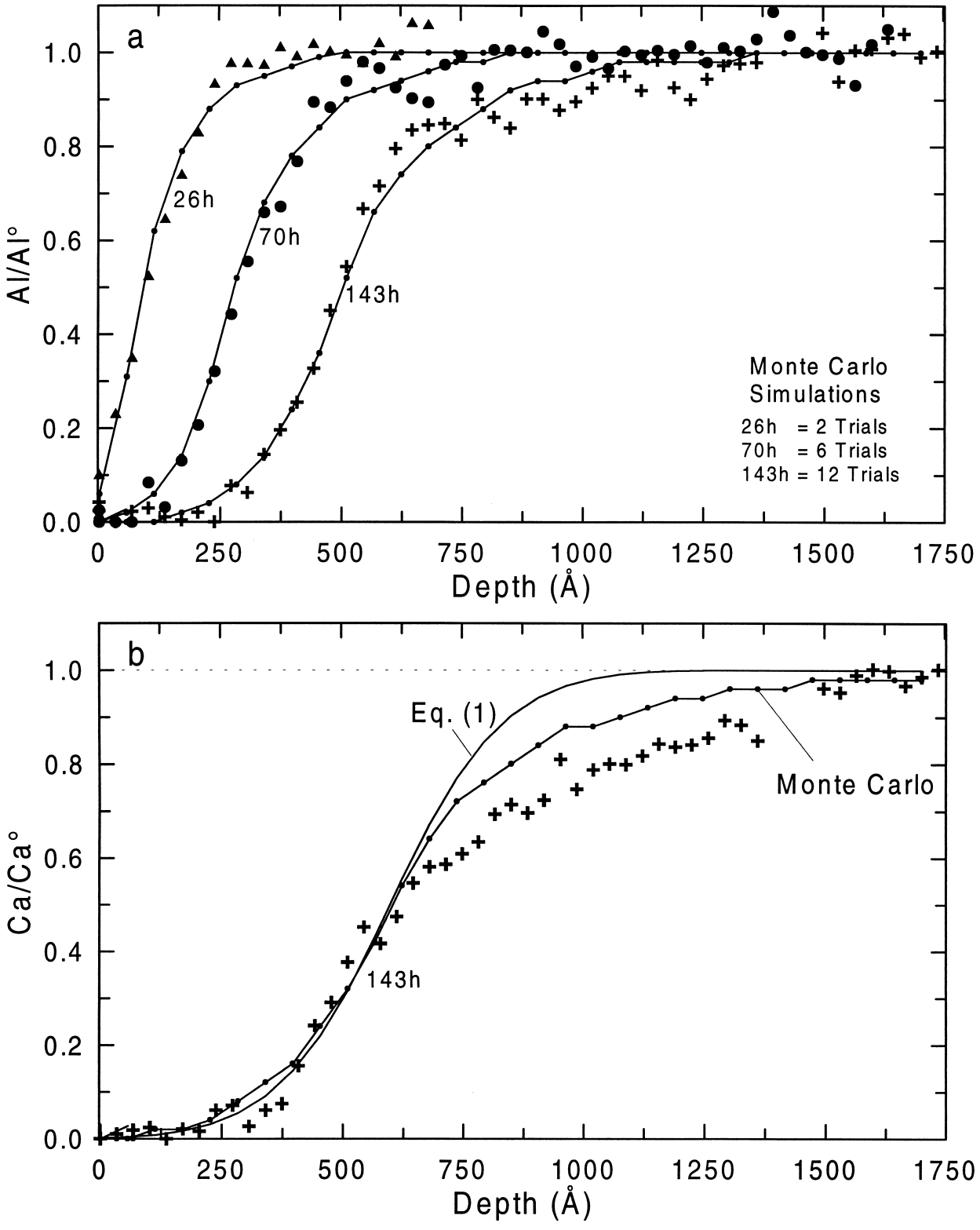

Fig. 7. XPS Al compositional depth profiles of labradorite (001) cleavage surfaces leached for 12 h (dots) and 48 h (crosses). (a) Simulations of the Al gradients, using a mathematical solution [Eqn. (2)] to the diffusion equation, are illustrated as solid curves. The solution is from Crank (1957). (b) Simulations of the Al gradients, using Monte Carlo calculations, are illustrated by the segmented lines joining the small dots.

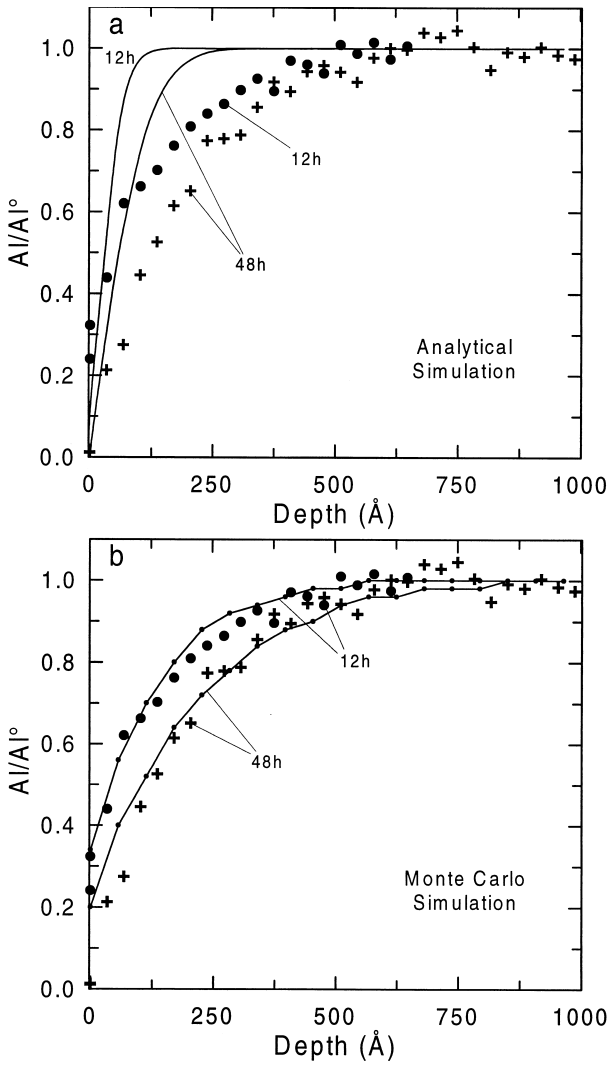

Fig. 8. XPS Ca compositional depth profiles of labradorite (001) cleavage surfaces leached by HCl solution of pH = 2.0. (a) Ca compositional gradients for 26 h (triangles), 70 h (dots), and 143 h (crosses) leaching. Simulations using a mathematical solution [Eqn. (1)] are plotted as smooth curves and coefficients are provided on the diagram. A Monte Carlo simulation of the 143 h data is plotted as small dots (discrete results) joined by straight line segments. (b) Ca compositional gradients for 12 h (triangles) and 48 h (dots) are plotted. Simulations using a mathematical solution [Eqn. (2)] are plotted as curves and coefficients used for the simulations are provided on the diagram.

simulations deviate appreciably from the experimental data. Due to photoelectron escape depths, the XPS Al analyses are depth-averaged values extending over about 30 Å, whereas the analytical solution calculates concentrations for an infinitely thin plane; consequently the XPS data necessarily yield a larger value than the simulation at depth.

7.2. Monte Carlo Simulation

A Monte Carlo simulation was conducted to determine if impeded diffusion accounts for the discrepancy. The solution–solid interface was taken as a stationary boundary. All sites of the feldspar (Fig. 4a, medium *B*) were initially occupied and the solution was initially considered to be devoid of aqueous cations. To approximate the great disparity in diffusion coefficients in solution and feldspar, it was assumed that once an atom was released to solution it immediately diffused into an infinitely large reservoir, thus $C_i(\text{aq}) = 0$ initially and for the duration of the simulation. Other aspects were the same as for the previous simulation (Fig. 7a).

The Monte Carlo compositional gradients are plotted in Figure 8b as segmented lines joining dots. The calculated Monte Carlo gradients better simulate the data than those calculated from Eqn. (2), suggesting again that impeded diffusion has substantial impact on gradients near the leaching front.

The Monte Carlo simulations yield Al/Al° interface values of about 0.32 and 0.20 for the 12 h and 48 h simulations (Fig. 8b). These are somewhat larger than measured (0.27 and 0.01, respectively). Chou and Wollast (1985) and Wollast and Chou (1992) demonstrate that exchange is an important initial reaction and it may account for the discrepancy. As well, the data of Figure 8b represent feldspar leached for 12 h and 48 h, the Monte Carlo trials were only doubled (rather than quadrupled) to simulate the two sets of data of Figure 8. Because the essential validity of the Monte Carlo formulation is proved by successfully simulating Al compositional profiles from 26 to 143 h leaching (Fig. 7a), we suggest that the Al diffusion coefficient decreases by half between 12 h and 26 h leaching; that is, leaching at 12 h is twice as fast as leaching between 26 h and 143 h. As explanation, H^+-metal ion exchange at the feldspar surface is extremely rapid (Chou and Wollast, 1985; Wollast and Chou, 1992). Because exchange was not included in the Monte Carlo simulation, the model underestimates diffusion rates during the formative leaching stage (less than 26 h). Detailed studies are required to understand this vital, initial stage of leaching.

8. CHARACTERISTICS OF NA GRADIENTS

Analysis of the pristine labradorite cleavage surface, before sputtering, indicates anomalously high Na values (Fig. 9) resulting perhaps from Na migration to the surface in response to cleavage or migration away from the surface in response to sputtering. Regardless, all leached surfaces yield low Na surface concentrations, indicating that Na, like Ca and Al is preferentially leached from the near surface. From these results it is apparent that Na behaves like Ca and Al during leaching. The software used to calculate the Na atomic percentages of Fig. 9 did not correct Na 2*s* intensities for the superimposed Al 2*p* satellite line (discussed previously), resulting in systematic overestimate of Na concentrations.

9. DISCUSSION AND CONCLUSIONS

9.1. Development and Evolution of Leached Zones

With initiation of leaching Al, Ca, and Na surface concentrations decrease producing compositional gradients which take on a convex-upward, hyperbolic aspect (Fig. 8). With time, the gradient evolves to assume a sigmoid shape (Fig. 4). With establishment of a sigmoid compositional gradient, three domains can be distinguished. One is the Si-rich domain where Na, Ca, and Al are effectively zero concentration (referred to as

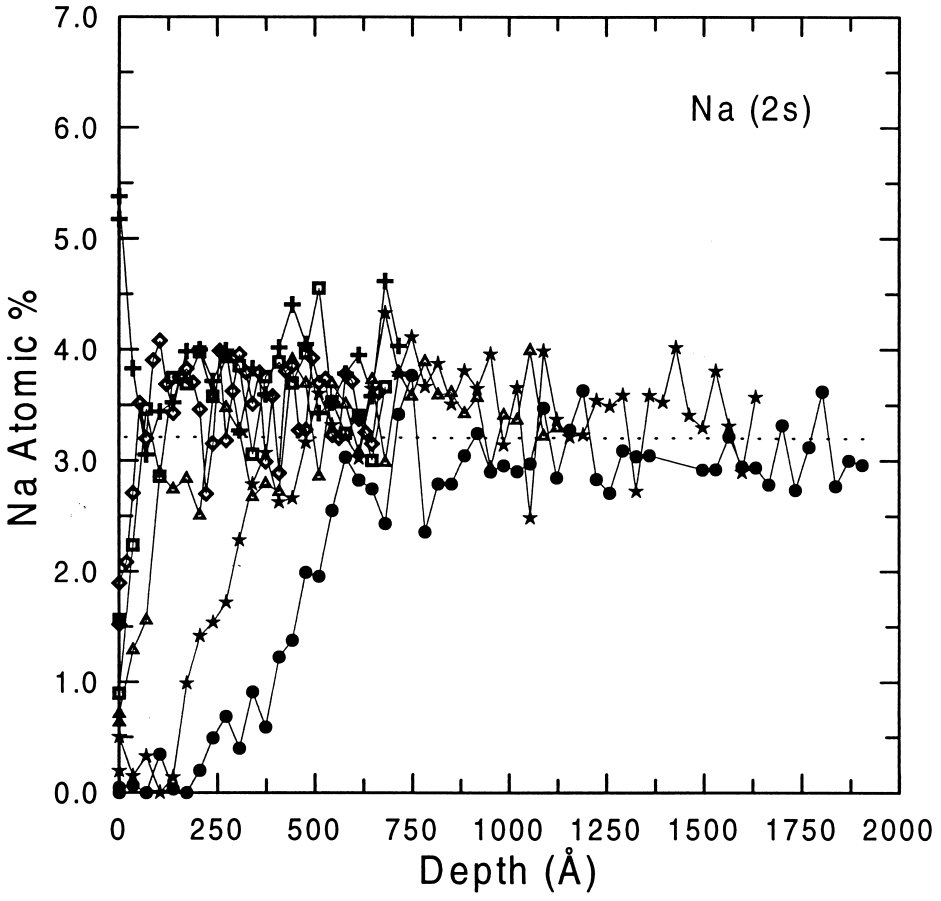

Fig. 9. XPS Na compositional depth profiles of labradorite (001) cleavage surfaces leached by HCl solution of pH = 2.0. Crosses represent Na compositions of an unreacted labradorite surface. Diamonds represent the gradient obtained after 12 h leaching, the squares, triangles, stars, and dots, represent, respectively, the compositional data collected after 26 h, 48 h, 70 h, and 143 h leaching. The data were collected using the Na 2*s* photopeak.

zone A), an active leaching zone in which the gradient takes on its sigmoid shape (zone B), and the unleached, bulk zone (zone C). The active leaching zone may be further subdivided into the leaching front where $C_i/C_i^0 > 0.5$ (zone B_1) and the tail where $C_i/C_i^0 < 0.5$ (zone B_2). These data may help in the effort to develop a much needed mathematical model for diffusive leaching, which both removes the mass balance restriction on the moving boundary approach here employed, and which accounts for impeded diffusion near the leaching front.

9.2. Properties of the Si-rich Zone (Zone A)

The Si-rich zone does not support measurable Al, Ca or Na compositional gradients (Fig. 4), yet these metals must migrate through this zone sufficiently rapidly to prevent high concentrations (measurable C_i/C_i^0 values); hence they must migrate at a rate at least commensurate with the rate of diffusion through zone B.

Repolymerization of the Si-rich zone (zone A) is extensive and may result in formation of distinct water-rich and siloxane-rich regions much like that observed for colloidal silica (Tomazawa and Capella, 1983; Casey et al., 1988; 1989; Westrich et al., 1990; Hellman et al., 1990). Such repolymerization produces water-rich regions 100's of Ångstrom in diameter (Casey and Bunker, 1990) so that diffusion coefficients in zone A may approach those in bulk solvent (H_2O).

9.3. Properties of the Active Leaching Zone (Zone B)

Equation (1) fails to mimic experimental data where Al/Al° > 0.8 and Ca/Ca° > 0.5 (Fig. 4). Application of this equation presumes that the diffusing element "Al," has equal probability to migrate in any direction (homogeneous medium with respect to diffusion). The Monte Carlo simulations which include "impeded" diffusion (element prevented from jumping to occupied structural sites) more accurately reproduce the experimental gradients than does Eqn. (1). This finding suggests that diffusion of Al and Ca is via structural sites (tetrahedral–tetrahedral) near the leaching front (close to the unreacted feldspar).

The diffusion coefficients of Al and Ca in zone B are, respectively, 2.5×10^{-17} and 4.0×10^{-17} cm^2/s. These are comparable to diffusion coefficients of K (5.9×10^{-17} cm^2/s) and Na (8.2×10^{-17} cm^2/s) in alkali silicate glasses (Frischat, 1975) and comparable with Mg in numerous silicates (Luce et al., 1972). The diffusion coefficients are, however, appreciably greater than diffusion coefficients of alkalis in bulk feldspar

(Lerman, 1979). As well, the results indicate that diffusion coefficients in zone A are at least 10^{-17} cm^2/s and may approach bulk solvent values (10^{-5} cm^2/s) if zone A segregates into water-like and siloxane-rich regions (Casey and Bunker, 1990).

Hydronium ion probably initiates dissolution of feldspars by diffusing into the mineral via sites interstitial sites. Its migration consequently should be largely independent of metal ion occupancy on cationic sites and dependent primarily on charge balance considerations. If ingress of hydrogen into the plagioclase is via interstitial sites, the analytical solution describing its diffusion into the mineral should be different from equations describing Al, Ca, and Na diffusion out of the mineral (via structural sites), but coupled through charge and mass balance considerations.

Acknowledgments—This paper benefited greatly from three reviews and especially Dr. A. Lerman who we especially thank for comments. We appreciate the enthusiastic discussions and encouragement provided by Roger Smart and Allan Pring. Experiments were conducted at Ian Wark Research Institute (IWRI, Adelaide, Australia). We thank the IWRI staff and administration for their support and good spirit. Special thanks are extended to Angus Netting who, in spite of our efforts, kept the XPS instrument running, and to Marek Zbik who performed the electron microprobe analyses. Funding to H.W.N. was provided by the National Science and Engineering Research Council of Canada.

REFERENCES

Adriaens A., Goossens D., Pijpers D., Van Tendeloo G., and Gijbels R. (1999) Dissolution Study of potassium feldspars using hydrothermally treated sanidine as an example. *Surf. Interface Sci.* **27,** 8–23.

Borg R. J. and Dienes G. J. (1992) *The Physical Chemistry of Solids*. Academic.

Briggs D. and Seah M. P. (1990) *Practical Surface Science. 1*. Wiley.

Casey W. H., Westrich H. R., and Arnold G. W. (1988) Surface chemistry of labradorite feldspar reacted with aqueous solutions at pH = 2, 3, and 12. *Geochim. Cosmochim. Acta* **52,** 2795–2807.

Casey W. H., Westrich H. R., Arnold G. W., and Banfield J. F. (1989) The surface chemistry of dissolving labradorite feldspar. *Geochim. Cosmochim. Acta* **53,** 821–832.

Casey W. H. and Bunker B. (1990) Leaching of mineral and glass surfaces during dissolution, in *Reviews in Mineralogy* (eds. M. F. Hochella and A. F. White), Vol. 23, pp. 397–426. Mineralogical Society of America.

Chou L. and Wollast R. (1985) Steady-state kinetics and dissolution mechanisms of albite. *Am. J. Sci.* **285,** 963–993.

Crank J. (1957) *The Mathematics of Diffusion*. Clarendon.

Danckwerts P. V. (1953) Continuous flow systems. *Chem. Eng. Sci.* **2,** 1–13.

Frischat G. H. (1975) *Ionic Diffusion in Oxide Glasses*. Diffusion and Defect Monograph Series, No. 3/4. Trans. Tech. Publications.

Hellman R., Eggleston C. M., Hochella M. F., and Crerar D. A. (1990) The formation of leached layers on albite surfaces during dissolution under hydrothermal conditions. *Geochim. Cosmochim. Acta* **54,** 1267–1281.

Kofstad P. (1972) *Nonstoichiometry, Diffusion, and Electrical Conductivity in Binary Metal Oxides*. Wiley-Interscience.

Le Claire A. D. and Ribanovitch A. (1984) The mathematical analysis of diffusion in dislocations. In *Diffusion in Crystalline Solids*. (eds. G. E. Murch and A. S. Nowick), pp. 257–318, Academic.

Lerman A. (1979) *Geochemical Processes Water and Sediment Environments*. Wiley Interscience.

Luce R. W., Bartlett R. W., and Parks G. A. (1972) Dissolution kinetics of magnesium silicates. *Geochim. Cosmochim. Acta* **36,** 35–50.

Muir I. J., Bancroft G. M., Shotyk W., and Nesbitt H. W. (1990) A SIMS and XPS study of dissolving plagioclase. *Geochim. Cosmochim. Acta* **54,** 2247–2256.

Muir I. J., Bancroft G. M., and Nesbitt H. W. (1989) Characteristics of altered labradorite surfaces by SIMS and XPS. *Geochim. Cosmochim. Acta* **53,** 1235–1241.

Muir I. J. and Nesbitt H. W. (1992) Controls on differential leaching of calcium and aluminium from labradorite in dilute electrolyte solutions. *Geochim. Cosmochim. Acta* **56,** 3979–3985.

Muir I. J. and Nesbitt H. W. (1997) Reactions of aqueous anions and cations at the labradorite-water interface: coupled effects of surface processes and diffusion. *Geochim. Cosmochim. Acta* **61,** 265–274.

Nesbitt H. W., MacRae N. D., and Shotyk W. (1991) Congruent and incongruent dissolution of labradorite in dilute, acidic, salt solutions. *J. Geol.* **99,** 429–442.

Schweda P., Sjoberg L., and Sodervall U. (1997) Near-surface composition of acid-leached labradorite investigated by SIMS. *Geochim. Cosmochim. Acta* **61,** 1985–1994.

Shewmon P. G. (1963) *Diffusion in Solids*. McGraw-Hill.

Shewmon P. G. (1969) *Transformations in Metals*. McGraw-Hill.

Smith J. V. and Brown W. L. (1987) *Feldspar Minerals*. Vol. 1. 2nd ed. Springer-Verlag.

Tomazawa M., and Capella S. (1983) Microstructure in hydrated silicate glass. *J. Am. Chem. Soc.* **66,** C24–C25.

Wagner C. D., Riggs W. M., Davis L. E., Moulder J. F., and Muilenberg G. E. (1976) *Handbook of X-ray Photoelectron Spectroscopy*. Physical Electronics.

Westrich H. R., Casey W. H., and Arnold G. W. (1990) Oxygen isotope exchange in the leached layer of labradorite feldspar. *Geochim. Cosmochim. Acta* **53,** 1681–1685.

Wollast R. and Chou L. (1992) Surface reactions during the early stages of weathering of albite. *Geochim. Cosmochim. Acta* **56,** 3113–3121.